ACRS 2022
MONGOLIA

QUALITY ASSESSMENT OF FUSED IMAGES BY VISUALIZATION OF UNCERTAINTY CHARACTERISTICS

Neema Nicodemus Lyimo[1]
[1]Sokoine University of Agriculture, College of Natural and Applied Sciences, Department of Informatics and Information Technology (DIIT), P.O.Box 3038, Morogoro, Tanzania,
Email: neemanico@sua.ac.tz

KEY WORDS: Quality assessment; uncertainty; fused images; medium resolution imagery; visualization

ABSTRACT: The geospatial community has benefited from open data initiatives in this Big Data era due to increasing availability of remote sensing data. However, mostly of the readily available imagery datasets are of low- to medium-resolution. Image fusion has been one of the common techniques to improve spatial and spectral resolution to support a majority of remote sensing applications. But, fusion results need to be evaluated before use for remote sensing applications. Both quantitative and qualitative (visual inspection) methods are used for assessment of the results. Moreover, visual examination of fused images has become a necessary procedure due to the sub-optimality of quantitative metrics. Visual inspection is can be done more effectively on high-resolution images, but it is more difficult on medium and low resolution images due to their coarseness. This paper proposes an approach to enhance visual assessment of fusion results for medium resolution imagery. The model provides a comprehensive evaluation of the uncertainty characteristics of the resulting images. Research findings prove that the proposed indices can effectively highlight the differences in fused images. Areas that have lost some spectral or spatial characteristics for a given fusion algorithm can be easily identified on the visualization layer than would otherwise be on the original results. The proposed approach has demonstrated a higher level of interpretation of the fusion results than single-valued quality metrics. The spatial explicit quality assessment model adds value, use, and acceptance of results derived from remote sensing products.

1. INTRODUCTION

Open data initiatives in this Big Data era have brought new and better services to the geospatial community. The available free remote sensing images are of low to medium resolution in which only homogenous areas can have pure pixels. Image fusion has been one of the preferred techniques to improve spatial and spectral resolution to support a majority of remote sensing applications. However, the fusion procedures are less than perfect. The least spectrally distorted image is the one that has not undergone any spatial enhancement. It has been emphasized in the literature that it is difficult to preserve both spectral and spatial information of the input images during fusion procedures (Dadrass Javan et al., 2021; Pohl, 2013; Snehmani et al., 2017). Due to the inherent difficulty in preserving the quality of both spectral and spatial information of the input images during fusion procedures, the quality assessment of fused images becomes an important topic in remote sensing.

Fused images need to be evaluated before use in remote sensing applications. Several quantitative metrics have been proposed including average gradient, the root mean squared error, the relative global synthesis error, correlation coefficient, to name a few. The earlier work by Wang and Bovik proved that the mean square error is inadequate for comparison with visual assessment of the results (Wang & Bovik, 2009). The findings have given rise to the definition of many other indexes for assessing image quality. The latest work by Shao applied ten indices as assessment metrics for their fusion results and concluded that no results can have all metrics optimal and that the process of fusion requires finding a balance between various metrics (Shao et al., 2020). A comparison assessment of different pan sharpening techniques using Landsat 8 imagery encountered the same contradictions when comparing best results according to statistical analysis and best results according to visual inspection (Govind et al., 2019). Despite the efforts, still, there is a lack of a universally accepted evaluation index matching the human capability in assessing the efficiency of fused results (Govind et al., 2019; Q. Wang et al., 2017). As a result, quality metrics for measuring image fusion quality and assessing the difference in quality between two images is still an open problem.

Due to sub-optimality of quantitative metrics visual inspection becomes a necessary complimentary procedure for assessment of fused images. Visual analysis of fused images is referred to as a qualitative method. This approach has an advantage of being simple; however, highly dependent on the visual conditions, viewers' experience, and sometimes it can be time-consuming (Jagalingam & Hegde, 2015; Wald et al., 1997). Visual inspection can be done more effectively in high-resolution, remotely sensed images; however, it is more challenging in medium and low resolution due to the coarse nature of the images. Therefore, this paper proposes an application of uncertainty model for enhancing image characteristics to facilitate quality assessment of the fusion results on medium resolution images.

The goal is to help the user to make an informed choice of a suitable fusion algorithm through visualization of uncertainties that can negatively affect the classification results.

2. METHODOLOGY

2.1 Study Area and Data

Our experiments used Landsat 8 data sets which cover a scene in Dodoma, the capital city of Tanzania (35.745°E, 6.171°S). The study area has a spatial extent of 1150 columns x 1030 rows of pixels of 30m Landsat bands. The city is in a semi-arid environment (Shemsanga et al., 2016). The study area is covered by urban buildings, roads (surfaced and unsurfaced roads), and dry areas with little /no vegetation, trees/shrub lands, farmlands, and water. Three popular pan-sharpened algorithms namely Brovey transform (BT), principal component analysis (PCA), and Gram–Schmidt (GS) spectral sharpening methods were applied to the multispectral images.

2.2 Method

Let's consider a classification task as the target application for the fused images. During fusion, changes that happen in the feature space and image space that may alter image characteristics to represent variations of the land cover surface. Hence modelling variations in both contexts provides a comprehensive understanding of image characteristics. Therefore, to improve the visual inspection of fusion results of medium resolution images, we model variations in the *feature space* and in the *image space (spatial domain)*.

2.2.1 Image Space Uncertainty (ISU)

High spatial heterogeneity and the level of detail in urban areas lead to intra-class spectral variability and mixed pixels. In a highly complex neighbourhood, there are greater variations in the local neighbourhood, than in a more homogenous area. A pixel that is so different from its neighbourhood has a higher chance of not belonging to the same class as its neighbourhood pixels. Hence, a pixel has high uncertainty when the difference with its neighbourhood is large (Zhang et al., 2019). A more complex region leads to higher uncertainties in the spatial domain. The secondary source of uncertainty is during image fusion. Processes such as resampling, interpolation calculations and matching involve approximations. Some uncertainty is introduced in the image space and feature space as well each time these procedures take place. Hence, the fused image is a result of a series of estimations.

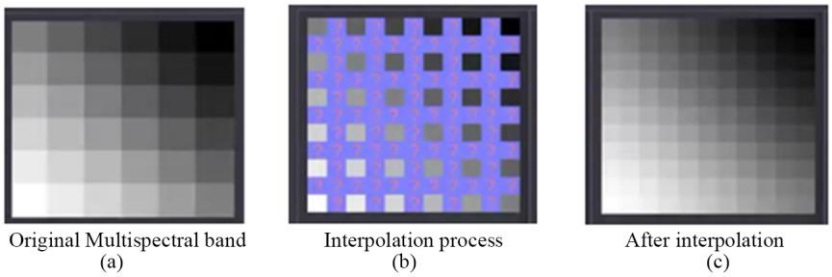

Figure 1.Changes taking place during image interpolation

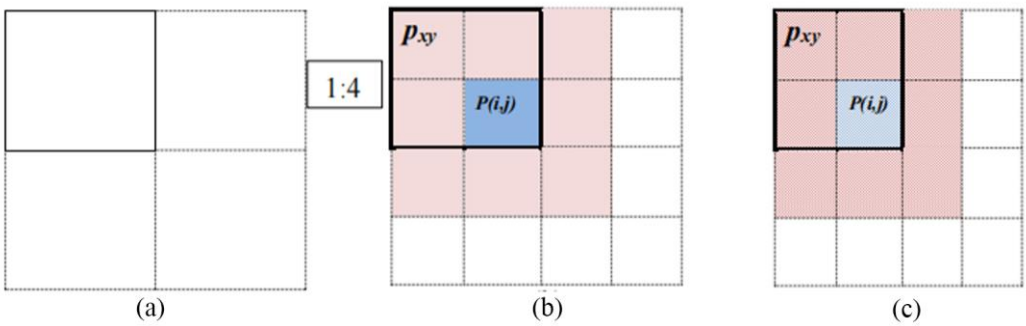

Figure 2. Changes in the image space a 3x3 pixel neighboring window

The square pixel neighboring window is referred to as *O(i,j)* with window length *l*. The size of the window is *lxl*, *Pxy* is the pixel of the x-th row and the y-th column in the *l*l* neighborhood, and a center pixel *P(i,j)*. For more reliable results I adapted the approach which favors the evaluation of fusion results at PAN scale (Alparone et al.,

2008)(Zhang, 2004)(Govind et al., 2019). I worked with a down-sampled multispectral image (MS) and a derived Pan sharpened image (PMS). Original MS image is *I*, resampled or interpolated image as *R*, and Pansharpened or fused image as *FI*.

Different bands have varied ability for modeling the environment; we can consider different bands as different features. For a k^{th} dimension feature in the multispectral space, spectral feature uncertainty of a pixel is high when the difference with its neighborhood is large. Spectral feature uncertainty (S) in a given neighborhood can be calculated using equation (*1*), (Zhang et al., 2019).

$$S_{p_{ij}}^{k} = \frac{\sum_{\forall p_{xy} \in O_{pij}^{k}} w_{p_{xy}} \cdot \left| f_{p_{xy}}^{k} - f_{p_{ij}}^{k} \right|}{l^2 - 1} \quad (1)$$

with $w_{p_{xy}}$ as the weight of influence of pixel P_{xy} on target pixel P_{ij} in the neighborhood window, the weight decreases with increasing distance from pixel P_{ij}, first law of geography (Lv et al., 2017). And, $f_{p_{xy}}$ and $f_{p_{ij}}$ are pixel values in the k^{th} feature that corresponds to pixels P_{xy} and P_{ij} in the kernel neighborhood window.

The ability of different bands for modeling the environment can be evaluated based on variations of the content of pixels in the given neighborhood. Locally adaptive weight provides better generalization than global weights (Lu et al., 2018). A study by Tsai et al. (2008) demonstrated that the amount of transmitted information based on information entropy is highly correlated to noise and blurring in medical imaging. Entropy has also been introduced in a recent work by Yu et al. (2020) to measure land cover heterogeneity. Both of these concepts are directly related to an increase in uncertainty. Hence, a Local Adaptive Multi-Feature Weighting Method based on Information Entropy theory is applied to measure feature uncertainty in both MS and PMS images.
Information entropy $E_{p_{ij}}^{k}$ of the local *l*l* neighborhood of pixel P_{ij} in the k^{th} band, can be computed as proposed in (Yu et al., 2020; Q. Zhang et al., 2019), in equation (2).

$$E_{p_{ij}}^{k} = -\sum_{\forall p_{xy} \in O_{pij}^{k}} P_{p_{xy}} \log_2 P_{p_{xy}} \quad (2)$$

$$P_{p_{xy}} = \frac{\left| f_{p_{xy}}^{k} - \frac{1}{l^2} \cdot \sum_{\forall p_{xy} \in O_{pij}^{k}} f_{p_{xy}}^{k} \right|}{\sum_{\forall p_{xy} \in O_{pij}^{k}} \left| f_{p_{xy}}^{k} - \frac{1}{l^2} \cdot \sum_{\forall p_{xy} \in O_{pij}^{k}} f_{p_{xy}}^{k} \right|} \quad (3)$$

Then, the overall uncertainty in image space will be given by equation 4.

$$S_{p_{ij}} = \sum_{k=1}^{K} S_{pij}^{k} \cdot E_{pij}^{k} \quad (4)$$

2.2.2 Feature Space Uncertainty (FSU)

In the feature space, pixels cluster together represents specific classes. Theoretically, the closer the pixels are to each other in the feature space, the more similar they are and the greater chance of belonging to the same class. In an ideal case, feature points in the feature space are highly concentrated around the cluster centre with clearly defined class boundaries, and we can have the highest confidence that these data fall under the same class. However, in reality, the distribution of points in the feature space will be more spread with varying degrees of uncertainty depending on the level of heterogeneity of the land cover. Feature points with high uncertainty will be those most affected by noise, mixed pixels, and intra-class differences. These points are frequently scattered far from cluster centres, increasing their chances of being misclassified.

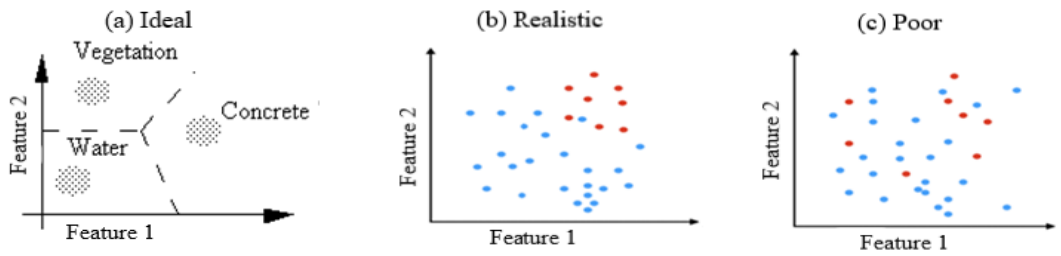

Figure 3. Distribution of feature points in the two-dimensional feature space

Quantitative assessments in the feature space are focused on the variations in the intensity distribution of feature points. In a pan-sharpened MS image, we are dealing with multiple clusters which need to be identified first. The more distant the two pixels are to each other for a given cluster in the feature space, the higher the uncertainty of belonging to the same information class and vice versa. Pixels belonging to a cluster with a higher concentration of pixels have lower uncertainty and vice versa. Therefore, centres of all clusters should be located at the high-density region of the feature points. Feature points that fall near the centre of high-density area in clusters will have lower uncertainty. In a cluster point that are far away from a high-density area are more likely not to belong in the same class. So, uncertainty increases as moving far away from high density area in clusters.

The distance between feature points in each cluster is determined by Euclidean spectral distance (ESD) equation (5):

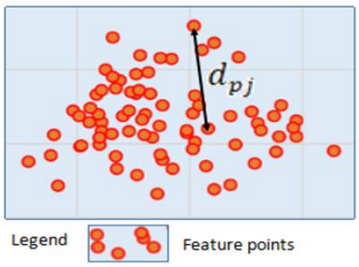

Figure 4. Example of calculating d_{pj}

$$d_{pj} = \sqrt{(f_p^k - f_j^k)^2} \quad (5)$$

with f_p^k representing the central reference feature point p with the highest local density in the cluster and f_j^k is the feature of the j^{th} pixel in the given cluster.
The density distribution of each cluster in a given layer is computed by the following equation 6:

$$\Phi_{C_k} = \frac{1}{m}\sum_{j=1}^{m} d_{pj} \quad (6)$$

where Φ_{C_k} represents distribution density of feature points in cluster c in band k; m is the total number of pixels representing the feature points for a given cluster c in band k; d_{pj} represents the ESD of the j[th] feature point to the cluster's reference centre point p. Then, we calculate the overall feature uncertainty for all layers by averaging the values of pixels from each band and refer to it as Φ_I.

2.2.3 Overall fusion uncertainty

Overall fusion uncertainty (FU) is obtained by taking the average measure of ISU and FSU.

2.2.4 Visualization and Validation Scheme

Rescaling of uncertainty values helps to make the difference in the results more visible for different fusion algorithms. Normalization is one of the common feature scaling methods, also referred to as dynamic range expansion. Dynamic range expansion has the benefit of bringing the image into a better range for image interpretation (Gonzalez & Woods, 2007). Therefore, the normalization transforms the uncertainty values (U) in the feature space and in the image space $U:\{\mathbb{X} \subseteq \mathbb{R}^n\} \longrightarrow \{Min, \dots, Max\}$ into a new image U_N: $\{\mathbb{X} \subseteq \mathbb{R}^n\} \longrightarrow \{newMin, \dots, newMax\}$.

An average of feature space and image space uncertainties provides a combined measure of uncertainty, *FU*. We are

using a common classification algorithm, Maximum likelihood classification (MLC). Each pixel is classified according to the class with the greatest probability. If the chance of the highest classification is less than the limit you set, the pixel stays unclassified. Therefore, we compute the discriminant functions for each pixel in the given image (Richards, 1999), to obtain the results for maximum likelihood classification. Furthermore, to test this phenomenon's validity, the uncertainty raster image (U) was reclassified into *N* desired levels. Then, Pearson correlation coefficient is used to determine the relationship between levels of uncertainty and the rate of unclassified pixels.

3. RESULTS & DISCUSSION

3.1 Uncertainty visualization results

Three fusion algorithms were applied, and their results are used for the assessment of the proposed model. The applied methods are Brovey transform (BT) pan-sharpening method, principal component analysis (PCA), and Gram–Schmidt (GS) spectral sharpening.

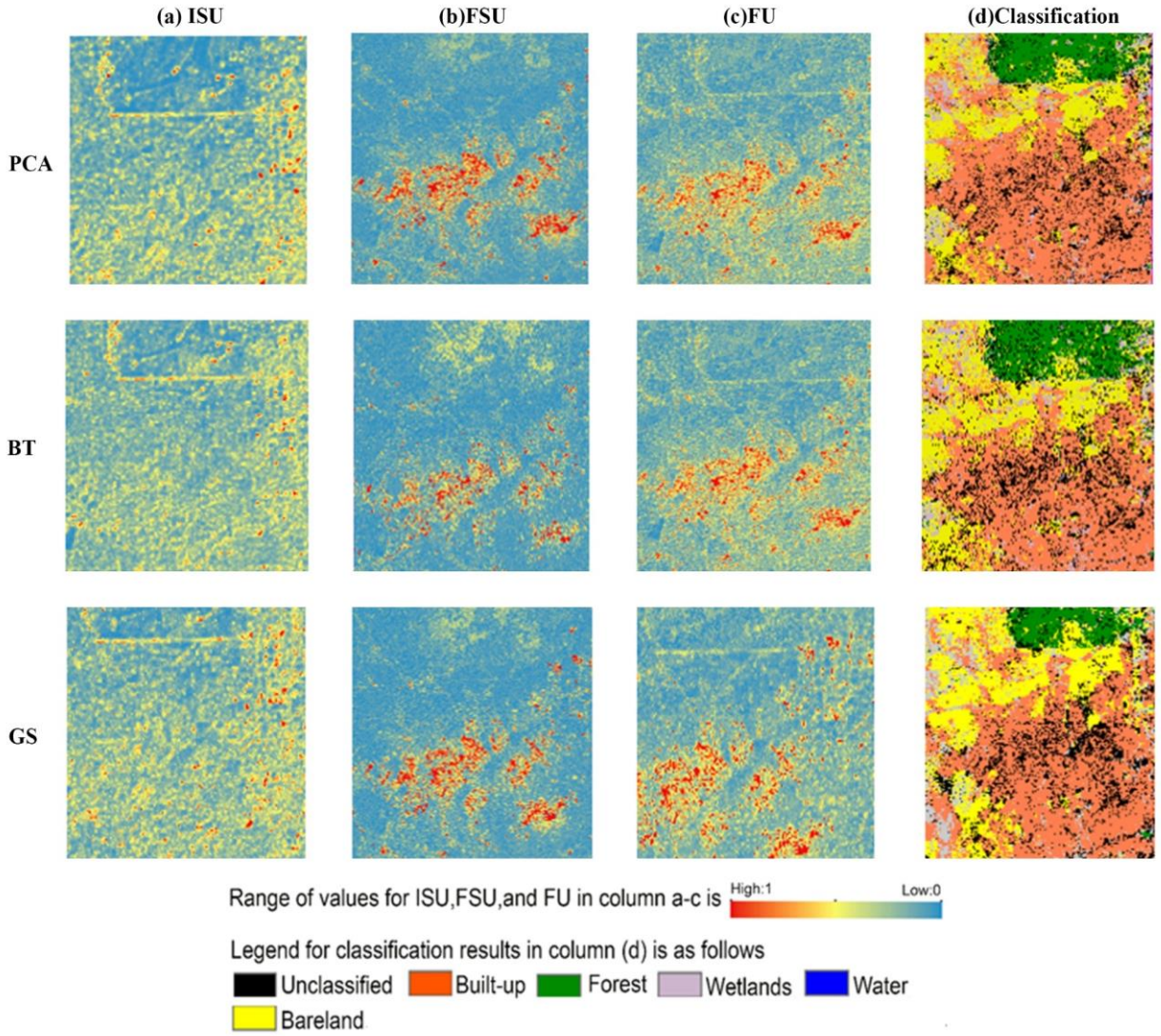

Figure 5. Results for image space uncertainty ISU, feature space uncertainty FSU, and overall uncertainty FU

The results of image-space uncertainty (ISU) and feature space uncertainty (FSU) of the pan-sharpened images were merged to form a fusion uncertainty index, FU. Results for ISU, FSU, and FU are as presented in Figure 7. The uncertainty indices were computed for the entire study area. After that, more investigation was carried out on areas that displayed significant variations. The results of classified images were used for statistical assessment of the corresponding uncertainty results. A corresponding section of classified images (column (d) in Figure 7) is used to assess the correlation.

3.2 Correlation Analysis

Parameters used for the proposed uncertainty approach are pixel neighbouring window size when calculating ISU, and the number of clusters when calculating feature space uncertainty. Five clusters were used to represent our study area classes based on visual inspection and literature recommendations (Yan et al., 2015). Several neighboring window sizes 3x3, 5x5, 7x7 and 9x9, have been tested and the number of classes was 5. The classification results were used for validation of the uncertainty model through correlation analysis.

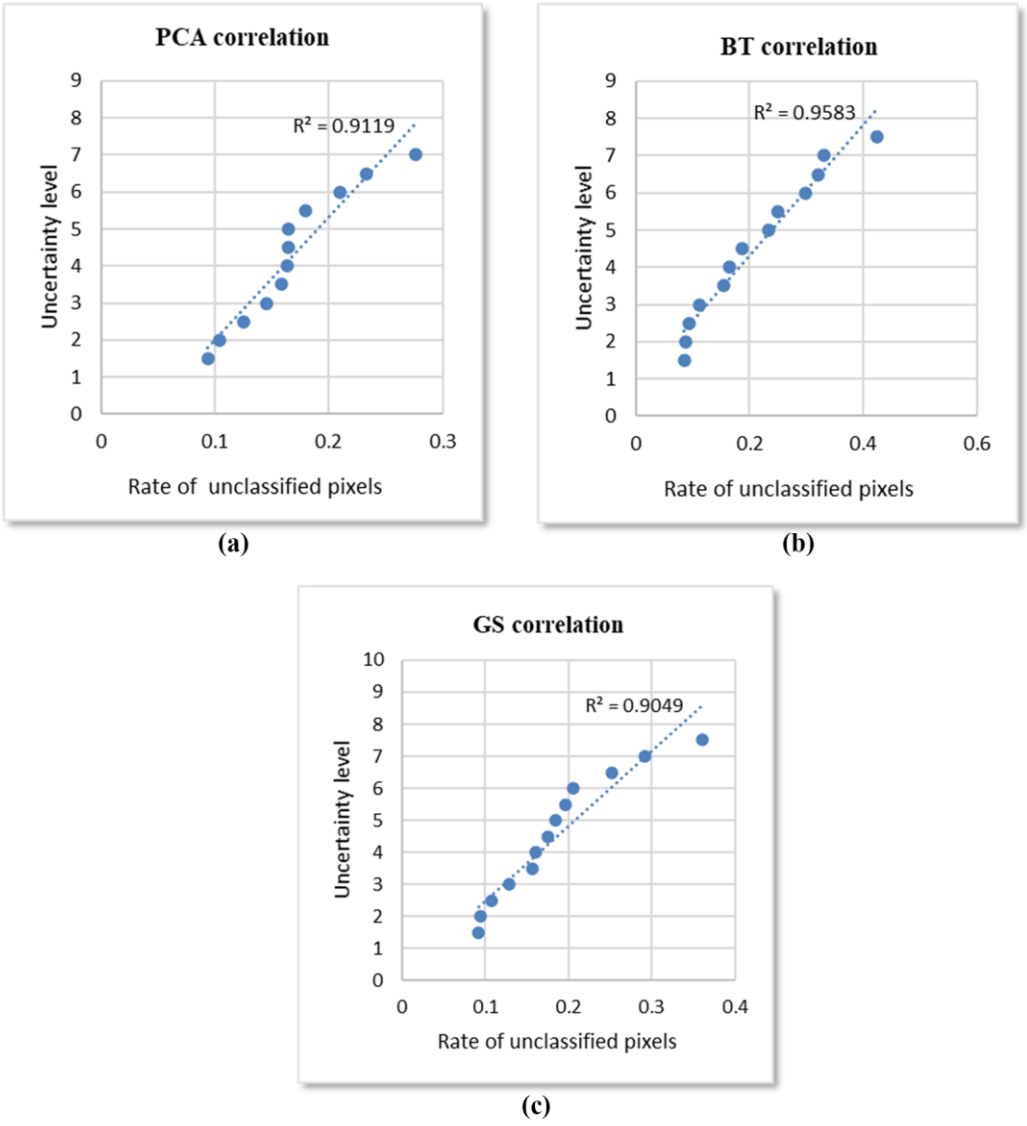

Figure 6. Scatterplots and fitted curves of the rate of unclassified pixels and the levels of uncertainty, for results in Figure 5

A class boundary for the MLC classifier was set to visualize areas with a high rate of unclassified pixels or a higher chance of misclassification. 0.1 class probability was assigned to all classes except for one; the forest class was assigned a probability of 0.6. These are parameters used for image classification with MLC. And, the values were set the same for all classification results. Uncertainty values for downscaled MS bands, pan-sharpened BT, PCA, and GS range from 0 – 1. Zero representing minimum uncertainty and one as maximum uncertainty. The probability of unclassified pixels for each corresponding uncertainty level was compared using the Pearson correlation coefficient, R. The scatterplots and fitted curves are displayed in Figure 6.

3.3 Assessment of the Proposed Model

The experimental results suggest that the proposed uncertainty model provides a good opportunity for enhanced visual inspection of medium-resolution fused images. Results demonstrate that the proposed indices can quantify and effectively create useful visualizations on how a fused image characterizes the scene's complexity. More complex areas have higher uncertainty and a higher rate of unclassified pixels, and vice versa. The correlation coefficient R between the uncertainty levels in the visualization map and the unclassified pixels rate is greater than 0.9 for all three tested cases in Figure 6. These findings promote applying the approach in practice, but the choice of parameters can influence the model's efficiency. Hence, the reason behind the selection of values for the given parameters must be known.

The lesson learned from parameter analysis is that the neighbourhood window size directly influences the correlation of the results. A very small kernel size like a 3x3 window is noisier, and it may raise unnecessary attention to very minor differences. The resulting image is also noisier. On the other hand, a very large window may suppress much of the uncertainties and limit the ability to visualize the difference in variations of image properties from one image to another. For visual assessment, we suggest a 7 by 7 kernel. This one provides a good visual presentation than the others, and at the same time, it can emphasize important differences in the images. The comparison analysis of kernel size used in the calculations of image space uncertainty and its influence on the overall correlation coefficients R is summarized in Table 1. Apart from the visualization aspect, a quantitative assessment of a 7x7 window yields the highest correlation as shown in Table 1.

A combination of ISU and FSU obtains overall uncertainty in the image. These indices complement each other. While FSU can be more affected by intra-class variations, ISU is also more sensitive to minor changes. Using an optimum neighbourhood window size is necessary to achieve the best ISU results. In some areas, ISU performed better than FSU, and vice versa. In this work, ISU and FSU had equal weight.

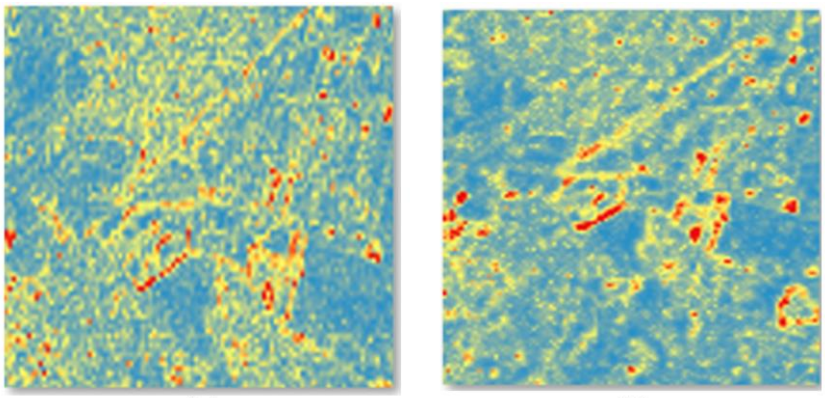

Figure 7. Results for GS based image space uncertainty (a) 3x3 neighbourhood window, and (b) 7x7 neighbourhood window

The model has performed very well for BT results in both cases. A more plausible explanation for this phenomenon could be its simplicity. BT uses RBG bands only, but PCA involves multiple bands and more complex transformations of the original vector space. GS algorithm is a generalization of PCA (Vivone et al., 2015). However, all three BT, GS, and PCA correlation results are good and satisfactory despite the minor differences.

Table 1. Comparison between neighborhood window size and correlation coefficient R

Fusion method	**Window size**	**Equations of the Fitted Curves**	**Correlation Coefficient *R***	***R*²**
PCA	3x3	y = 36.681x - 1.5002	0.909	0.8272
	7x7	y = 33.033x - 1.3051	0.954	0.9119
BT	3x3	y = 5.0683x + 1.8282	0.914	0.8354
	7x7	y = 17.534x + 0.7998	0.978	0.9583
GS	3x3	y = 21.598x + 0.6882	0.914	0.8363
	7x7	y = 23.4x + 0.1688	0.951	0.9049

3.4 Advantage of the visualization results in comparison with the traditional approaches

Over the years, several image fusion algorithms have been proposed. The reason behind such a proliferation of research work in this area is a challenging complexity trade-off for optimization of spatial and spectral parameters to provide superior results at minimal loss of image quality. Visual inspection has been recommended as a necessary procedure for identifying local spectral and spatial distortions in rendering details of the fused results (Alparone et al., 2007; Mas et al., 2017). The visualization indices proposed in this work have enhanced visual inspection of fusion results for medium resolution remotely sensed images.

Figure 8 illustrates the proposed model's results, and demonstrated how it highlights the differences between the images. These results can be interpreted as follows. Areas with high uncertainty inform us that these are areas of high complex neighbourhoods. In comparison, regions with low uncertainty are expected to be more homogenous and have more pixels which are similar to others in the region.

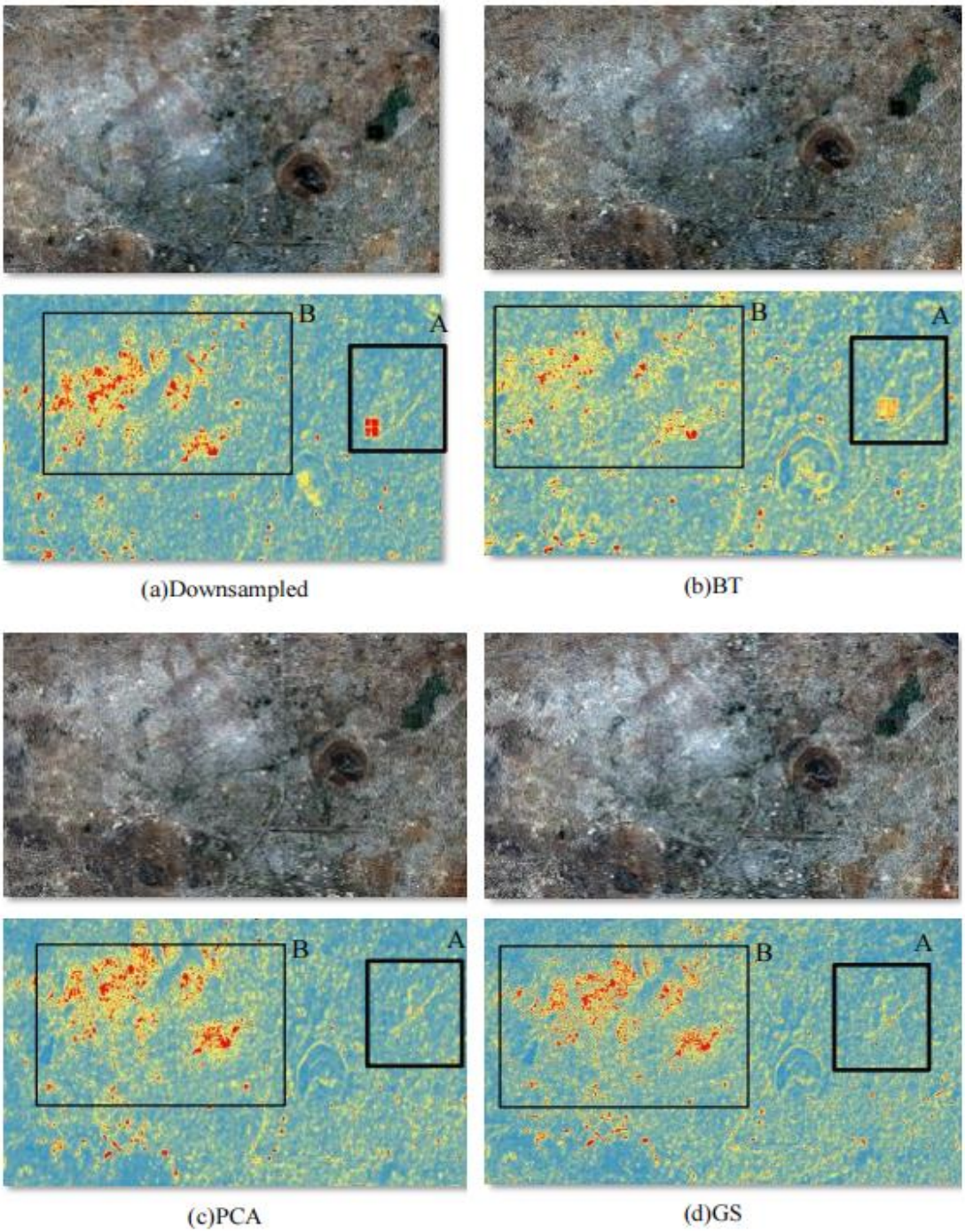

Figure 8. A comparison of fusion algorithms

In Figure 8, if a user's interest is to analyse a wastewater pond and its surroundings in A, BT results would be the best. Despite the fusion effects, still maintain some key features to delineate this area from the rest. However, PCA and GS result in this area exhibiting very low variations in this neighbourhood (square A). This result tells us that a fused image has lost some characteristics to efficiently discriminate between land cover classes in this area compared to BT results. However, in region B, PCA and GS maintain most land cover variations that BT in this area. It is more challenging to observe these differences in the fused images without the visualization layer's help. Visualization of the variations provides a helpful tool for visual inspection of fusion results of coarse images.

Another advantage proposed approach is that the visualization indices facilitate a high level of interpretation of fusion results. Single valued evaluation metrics such as RMSE, SAM, SNR have limited ability to help the analyst conceptualize characteristics of the resulting image (Hodgson, 1998). Single valued metrics are intended to report the accuracy of the entire image with a single value. Spatially explicit models can add value, use, and acceptance of results derived from remote sensing products (Foody & Atkinson, 2006; Samadzadegan, 2013). The proposed uncertainty model provides a better understanding of the quality of the resulting image for the intended application.

4. CONCLUSION

The selection of an appropriate fusion algorithm that maintains both spectral and spatial content in the fused image is challenging, a much-debated problem (Alparone et al., 2007). Due to the sub-optimality of existing quantitative evaluation procedures, a qualitative evaluation of the results through visual inspection is a necessary procedure (Vivone et al., 2015). Therefore, this paper put forward a visualization model for enhanced visual inspection of fusion results of medium resolution images. The index is an output of a comprehensive model that reveals the uncertainty characteristics in a fused image to represent land cover surface variations or complexity. Best fusion results of a high complex neighbourhood in the visualization model reveals higher variations of the given area otherwise the results are considered less reliable, and the vice versa. Results of the validation experiments in this paper show a high correlation in all tested cases encouraging the application of the model in practice.
The results of the model provide a higher level of interpretation of fusion results compared to single-valued quantitative metrics. Furthermore, the visualization layers have proved to reveal key uncertainty characteristics that would otherwise be difficult to observe by visual inspection of fusion results only in the case of medium satellite images. In this paper, however, uncertainty has been assessed at a pixel level. Due to high generalization in coarse resolution, some aspects of uncertainties may not be easily mapped at a pixel level. Future works may focus on sub-pixel uncertainty models for the evaluation of fused images.

REFERENCES

Alparone, L., Aiazzi, B., Baronti, S., Garzelli, A., Nencini, F., & Selva, M. 2008. Multispectral and panchromatic data fusion assessment without reference. *Photogrammetric Engineering and Remote Sensing*, *74*(2), 193–200. https://doi.org/10.14358/PERS.74.2.193

Alparone, L., Wald, L., Chanussot, J., Thomas, C., Gamba, P., & Bruce, L. M. 2007. Comparison of pansharpening algorithms: Outcome of the 2006 GRS-S data-fusion contest. *IEEE Transactions on Geoscience and Remote Sensing*, *45*(10), 3012–3021. https://doi.org/10.1109/TGRS.2007.904923

Dadrass Javan, F., Samadzadegan, F., Mehravar, S., Toosi, A., Khatami, R., & Stein, A. 2021. A review of image fusion techniques for pan-sharpening of high-resolution satellite imagery. *ISPRS Journal of Photogrammetry and Remote Sensing*, *171*(November 2020), 101–117. https://doi.org/10.1016/j.isprsjprs.2020.11.001

Foody, G. M., & Atkinson, P. M. 2006. Uncertainty in Remote Sensing and GIS. In *Uncertainty in Remote Sensing and GIS*. https://doi.org/10.1002/0470035269

Gonzalez, R. C., & Woods, R. E. 2007. Digital Image Processing (3rd Edition). In *Prentice-Hall, Inc. Upper Saddle River, NJ, USA ©2006*.

Govind, N. R., Rishikeshan, C. A., & Ramesh, H. 2019. Comparison of Different Pan Sharpening Techniques using Landsat 8 Imagery. *2019 IEEE 5th International Conference for Convergence in Technology, I2CT 2019*, *Figure 2*, 1–4. https://doi.org/10.1109/I2CT45611.2019.9033659

Hodgson, M. E. 1998. *1998_Aug_797-807.Pdf*. *8*, 797–807.

Jagalingam, P., & Hegde, A. V. 2015. A Review of Quality Metrics for Fused Image. *Aquatic Procedia*, *4*(Icwrcoe), 133–142. https://doi.org/10.1016/j.aqpro.2015.02.019

Lu, X., Wang, J., Li, X., Yang, M., & Zhang, X. 2018. An adaptive weight method for image retrieval based

multi-feature fusion. *Entropy*, *20*(8). https://doi.org/10.3390/e20080577

Lv, Z., Zhang, P., & Benediktsson, J. A. 2017. Automatic object-oriented, spectral-spatial feature extraction driven by Tobler's first law of geography for very high resolution aerial imagery classification. *Remote Sensing*, *9*(3). https://doi.org/10.3390/rs9030285

Mas, J. F., Lemoine-Rodríguez, R., González-López, R., López-Sánchez, J., Piña-Garduño, A., & Herrera-Flores, E. 2017. Land use/land cover change detection combining automatic processing and visual interpretation. *European Journal of Remote Sensing*, *50*(1), 626–635. https://doi.org/10.1080/22797254.2017.1387505

Pohl, C. 2013. Challenges of Remote Sensing Image Fusion to Optimize Earth Observation Data Exploration. *European Scientific Journal*, *4*(December), 355–365. http://eujournal.org/index.php/esj/article/download/2487/2360

Richards, J. A. 1999. *Remote Sensing Digital Image Analysis*. Springer-Verlag.

Samadzadegan, F. 2013. *Image Fusion Quality Assessment of High Resolution Satellite Imagery based on an Object Level Strategy*. *7*, 140–148.

Shao, Z., Wu, W., & Guo, S. 2020. IHS-GTF: A fusion method for optical and synthetic aperture radar data. *Remote Sensing*, *12*(17), 1–20. https://doi.org/10.3390/rs12172796

Shemsanga, C., Muzuka, A. N. N., Martz, L., Komakech, H., & Omambia, A. N. 2016. Statistics in climate variability, dry spells, and implications for local livelihoods in semiarid regions of Tanzania: The way forward. In *Handbook of Climate Change Mitigation and Adaptation, Second Edition* (Vol. 2, pp. 801–848). Springer International Publishing. https://doi.org/10.1007/978-3-319-14409-2_66

Snehmani, Gore, A., Ganju, A., Kumar, S., Srivastava, P. K., & Hari Ram, R. P. 2017. A comparative analysis of pansharpening techniques on quickbird and WorldView-3 images. *Geocarto International*. https://doi.org/10.1080/10106049.2016.1206627

Tsai, D. Y., Lee, Y., & Matsuyama, E. 2008. Information entropy measure for evaluation of image quality. *Journal of Digital Imaging*, *21*(3), 338–347. https://doi.org/10.1007/s10278-007-9044-5

Vivone, G., Alparone, L., Chanussot, J., Mura, M. D., Garzelli, A., Member, S., Licciardi, G. A., Restaino, R., & Wald, L. 2015. *Pansharpening Algorithms*. *53*(5), 2565–2586.

Wald, L., Ranchin, T., & Mangolini, M. 1997. Fusion of satellite images of different spatial resolutions: Assessing the quality of resulting images. *Photogrammetric Engineering and Remote Sensing*, *63*(6), 691–699.

Wang, Q., Blackburn, G. A., Onojeghuo, A. O., Dash, J., Zhou, L., Zhang, Y., & Atkinson, P. M. 2017. Fusion of Landsat 8 OLI and Sentinel-2 MSI Data. *IEEE Transactions on Geoscience and Remote Sensing*, *55*(7), 3885–3899. https://doi.org/10.1109/TGRS.2017.2683444

Wang, Z., & Bovik, A. C. 2009. Mean squared error: Lot it or leave it? A new look at signal fidelity measures. *IEEE Signal Processing Magazine*, *26*(1), 98–117. https://doi.org/10.1109/MSP.2008.930649

Yan, W. Y., Shaker, A., & El-Ashmawy, N. 2015. Urban land cover classification using airborne LiDAR data: A review. In *Remote Sensing of Environment*. https://doi.org/10.1016/j.rse.2014.11.001

Yu, J., Peng, S., Zhang, W., & Kang, S. 2020. Index for the consistent measurement of spatial heterogeneity for large-scale land cover datasets. *ISPRS International Journal of Geo-Information*, *9*(8). https://doi.org/10.3390/ijgi9080483

Zhang, Q., Zhang, P., & Xiao, Y. 2019. A modeling and measurement approach for the uncertainty of features extracted from remote sensing images. *Remote Sensing*, *11*(16). https://doi.org/10.3390/rs11161841

Zhang, Y. (2004). Understanding image fusion. *Photogrammetric Engineering and Remote Sensing*, *70*(6), 657–661.